NIH Public Access
Author Manuscript
J Am Chem Soc. Author manuscript; available in PMC 2013 October 24.

Published in final edited form as:
J Am Chem Soc. 2012 October 24; 134(42): 17526–17535. doi:10.1021/ja304525n.

Assembly and Properties of Heterobimetallic $Co^{II/III}/Ca^{II}$ Complexes with Aquo and Hydroxo Ligands

David C. Lacy[†], **Young Jun Park**[†], **Joseph W. Ziller**[†], **Junko Yano**[¶], and **A. S. Borovik**[†,*]

[†]Department of Chemistry, University of California-Irvine, 1102 Natural Sciences II, Irvine, CA 92697

[¶]Physical Bio-sciences Division, Lawrence Berkeley National Laboratory, Berkeley, CA 94720

Abstract

The use of water as a reagent in redox-driven reactions is advantageous because it is abundant and environmentally compatible. The conversion of water to dioxygen in photosynthesis illustrates one example, in which a redox-inactive Ca^{II} ion and four manganese ions are required for function. In this report we describe the stepwise formation of two new heterobimetallic complexes containing $Co^{II/III}$ and Ca^{II} ions, and either hydroxo or aquo ligands. The preparation of a 4-coordinate Co^{II} synthon was achieved with the tripodal ligand, *N,N′,N″*-[2,2′,2″-nitrilotris(ethane-2,1-diyl)]tris(2,4,6-trimethylbenzenesulfonamido, $[MST]^{3-}$. Water binds to $[Co^{II}MST]^{-}$ to form the 5-coordinate $[Co^{II}MST(OH_2)]^{-}$ complex that was used to prepare the Co^{II}/Ca^{II} complex $[Co^{II}MST(\mu\text{-}OH_2)Ca^{II}\subset 15\text{-crown-}5(OH_2)]^{+}$ ($[Co^{II}(\mu\text{-}OH_2)Ca^{II}OH_2]^{+}$). $[Co^{II}(\mu\text{-}OH_2)CaOH_2]^{+}$ contained two aquo ligands, one bonded to the Ca^{II} ion and one bridging between the two metal ions and thus represents an unusual example of a heterobimetallic complex containing 2 aquo ligands spanning different metal ions. Both aquo ligands formed intramolecular hydrogen bonds with the $[MST]^{3-}$ ligand. $[Co^{II}MST(OH_2)]^{-}$ was oxidized to form $[Co^{III}MST(OH_2)]$ that was further converted to $[Co^{III}MST(\mu\text{-}OH)Ca^{II}\subset 15\text{-crown-}5]^{+}$ ($[Co^{III}(\mu\text{-}OH)Ca^{II}]^{+}$) in the presence of base and $Ca^{II}OTf_2$/15-crown-5. $[Co^{III}(\mu\text{-}OH)Ca^{II}]^{+}$ was also synthesized from the oxidation of $[Co^{II}MST]^{-}$ with PhIO in the presence of $Ca^{II}OTf_2$/15-crown-5. Allowing $[Co^{III}(\mu\text{-}OH)Ca^{II}]^{+}$ to react with diphenylhydrazine afforded $[Co^{II}(\mu\text{-}OH_2)Ca^{II}OH_2]^{+}$ and azobenzene. Additionally, the characterization of $[Co^{III}(\mu\text{-}OH)Ca^{II}]^{+}$ provides another formulation for the previously reported Co^{IV}–oxo complex, $[(TMG_3tren)Co^{IV}(\mu\text{-}O)Sc^{III}(OTf)_3]^{2+}$ to one that instead could contain a Co^{III}–OH unit.

INTRODUCTION

A significant challenge in synthetic chemistry is regulating the secondary coordination sphere of metal ion(s) to affect function.[1] These types of regulatory interactions are found within the active sites of metalloproteins and aid in promoting efficient and selective transformations. Non-covalent interactions are the major forces that control the properties of the secondary coordination spheres in proteins. For instance, intramolecular hydrogen bonds (H-bonds) involving metal bound water ligands are often found within the structures of active sites and are instrumental in dictating subsequent function. Lipoxygenase is a non-heme iron enzyme that catalyzes the cleavage of C–H bonds by cycling between Fe^{III}–OH and Fe^{II}–OH_2 states.[2] In both states, it is proposed that H-bonding networks involving the

Corresponding Author: aborovik@uci.edu.

ASSOCIATED CONTENT

Crystallographic details for all the molecular structures with CIFs, and Figures S1–S9. This material is available free of charge via the Internet at http://pubs.acs.org.

NIH-PA Author Manuscript
NIH-PA Author Manuscript
NIH-PA Author Manuscript

NIH-PA Author Manuscript

NIH-PA Author Manuscript

NIH-PA Author Manuscript

hydroxo/aquo ligands are necessary for catalysis. Additionally, recent structural evidence on the oxygen-evolving complex (OEC) within Photosystem II has shown that the active site contains an extensive H-bonding network surrounding the terminal aquo ligands on the Mn_4CaO_5 cluster that most likely influences function.[3,4] The OEC also illustrates that calcium ions have an essential role in the oxidation of water to dioxygen.[5] The presence of a Ca^{II} ion within the OEC cluster suggests that group 2 metal ions can influence other redox processes performed by transition metal complexes. In fact, synthetic molecular water oxidation catalysts often contain a mixture of transition metal ions and group 1 or 2 ions,[6a] such as in the cobalt/K_3PO_4 system developed by Kanan and Nocera.[6b,c] Recent examples of MnCaO clusters have also been reported; in particular, the Mn_3CaO_4 system of Agapie demonstrated the role of the Ca^{II} ion in modulating redox potentials.[7,8] Nevertheless, the limited number of discrete molecular examples makes it difficult to assess the effects of H-bonds and group 2 metal ions on redox processes at transition metal ions. Moreover, there are few synthetic examples of heterometallic complexes containing aquo ligands bound similarly to those found in the OEC.

In this report we describe the stepwise assembly of a series of $Co^{II/III}$–OH_2 and Co^{III}–OH complexes from water that contain intramolecular H-bonds and Ca^{II} ions (Chart 1). The complexes are formed using the tripodal ligand *N,N′,N″*-[2,2′,2″-nitrilotris(ethane-2,1-diyl)]tris-(2,4,6-tri-methylbenzenesulfonamido) ($[MST]^{3-}$) that contains three sulfonamido units. We have shown that this design supports formation of complexes with (Ca^{II}-(μ-OH)-Mn^{III}) cores.[9] The formation of the heterobimetallic Ca/Co complexes in the present study establishes the importance of Ca^{II} ions in stabilizing water binding and is crucial in activating the cobalt center for redox chemistry. Moreover, our findings suggest that the recently reported heterobimetallic $[(TMG_3tren)Co^{IV}(\mu\text{-}O)Sc^{III}(OTf)_3]^{2+}$ complex could be formulated to have a Co^{III}–OH unit rather than the more unusual Co^{IV}–oxo moiety.[10]

EXPERIMENTAL SECTION

General Methods

All reagents were purchased from commercial sources and used as received, unless otherwise noted. Solvents were sparged with argon and purified using a JC Meyer Co. solvent system. Potassium hydride (KH) as a 30% dispersion in mineral oil was filtered with a medium porosity glass frit and washed 5 times each with pentane and Et_2O. Solid KH was dried under vacuum and stored under an inert atmosphere. The syntheses of metal complexes were conducted in a Vacuum Atmospheres, Co. drybox under an argon atmosphere. The ligand H_3MST,[9] $Ca(OTf)_2$/15-crown-5,[9] $[FeCp_2]OTf$,[11a] acetyl ferrocenium tetrafluoroborate,[11b] and $Ca^{II}[N(TMS)_2]_2THF_2$,[11c] and PhIO[11d] were synthesized according to literature methods. Tetrabutylammonium hexafluorophosphate (TBAP) was recrystallized from hot ethanol 3 times and dried at 150°C for several days under reduced pressure.

Preparative Methods

Preparation of $Me_4N[Co^{II}MST]$—H_3MST (900 mg, 1.3 mmol) was dissolved in 45 mL of DMA, and KH (160 mg, 3.9 mmol) was added and allowed to stir until gas evolution ceased (~30 min). This solution was allowed to react with $Co^{II}(OAc)_2$ (230 mg, 1.3 mmol) and $Me_4N(OAc)$ (260 mg, 1.9 mmol), and the mixture was allowed to stir overnight. The resulting purple solution was filtered to remove insoluble white material (KOAc, 330 mg, 3.4 mmol, 94% yield), the purple filtrate was concentrated (~5 mL), and Et_2O was added to form a precipitate. The resulting blue solid was isolated on a fritted-glass funnel, washed several times with Et_2O, and dried under vacuum for several hours (990 mg, 93%). Further purification of the crude material was possible by dissolving the blue solid in DCM and

NIH-PA Author Manuscript

NIH-PA Author Manuscript

NIH-PA Author Manuscript

layering under pentane (660 mg, 62%). Dissolving the crude blue salt in a DMA and MeCN mixture (1:1) and allowing for slow vapor diffusion of Et_2O afforded crystals suitable for X-ray diffraction analysis. FTIR: (KBr, cm^{-1}) selected vibrations 3039, 3021, 2975, 2935, 2874, 2854, 2838, 1655, 1604, 1563, 1488, 1467,1446, 1405, 1379, 1346, 1279, 1237, 1221, 1141, 1102, 1073, 1055, 1039, 975, 960, 943, 932, 847, 826. UV–vis: λ_{max} (DCM, nm (ε, $M^{-1}cm^{-1}$)) 420 (shoulder), 410 (23), 568 (72), 752 (14). Solid suitable for elemental analysis was recrystallized from DCM/pentane. Anal. Calcd (found) for $Me_4N[Co^{II}MST]$ ·0.25 DCM ($C_{37.25}H_{57.5}Cl_{0.5}CoN_5O_6S_3$): C, 52.99 (52.68); H, 6.86 (6.91); N, 8.30 (8.33). An alternative method was also utilized: crystalline solid of this salt could be obtained by slow diffusion of Et_2O into the initial DMA filtrate, which after 4 days yielded sky blue crystals (780 mg, 73%).

Preparation of $Me_4N[Co^{II}MST(OH_2)]$—$Me_4N[Co^{II}MST]$ (99 mg, 0.12 mmol) was dissolved in DCM (~5 mL) and treated with water (20 μL, 1.11 mmol), and the sky blue solution turned pink. Layering the pink solution under pentane produced a crystalline solid of the salt. The pink micro-crystals were isolated by decanting and then dried by flowing Ar over the solid for a few seconds (prolonged drying or use of vacuum resulted in loss of the aquo ligand). FTIR: (Nujol, cm^{-1}) ν(OH) 3494, 3186; (KBr, cm^{-1}) ν(OH) 3602, 3497, 3273; selected vibrations (KBr, cm^{-1}) 3022, 2960, 2913, 2856, 1653, 1603, 1563, 1489, 1467, 1451, 1405, 1377, 1384, 1256, 1231, 1133, 1120, 1093, 1055, 1038, 978, 957, 932, 846, 826, 813. UV–Vis: λmax (DCM, nm (ε, $M^{-1}cm^{-1}$)) 530 (63), 712 (26). Anal. Calcd (found) for $Me_4N[Co^{II}MST(OH_2)]\cdot 2H_2O$ ($C_{37}H_{63}CoN_5O_9S_3$): C, 50.67 (50.73); H, 7.24 (7.18); N, 7.99 (7.79)

Preparation of $[Co^{II}MST(\mu\text{-}OH_2)Ca^{II}\subset 15\text{-crown-}5\text{-}(OH_2)]OTf$—$Me_4N[Co^{II}MST]$ (100 mg, 0.13 mmol) was dissolved in 4 mL of DCM and $Ca^{II}OTf_2$/15-crown-5 (73 mg, 0.13 mmol) was added. After stirring for 5 min, the homogenous blue solution was treated with water (12 mg, 0.67 mmol) and the solution turned pink. Crystals suitable for diffraction were obtained by layering the pink solution under pentane. Crystallized compound was separated from Me_4NOTf by vigorously stirring with pentane and decanting; the pink salt was isolated on a fritted-glass funnel and dried under reduced pressure (111 mg, 63%). FTIR: (Nujol, cm^{-1}) ν(OH) 3430 and 3218; selected vibrations 1604, 1564, 1151, 1124, 1096, 1033, 992, 980, 955, 892, 875, 819. UV–vis: λ_{max} (DCM, nm (ε, $M^{-1}cm^{-1}$)) 530 (49), 698 (28). Anal. Calcd (found) for $[Co^{II}MST(\mu\text{-}OH_2)Ca\subset 15\text{-crown-}5(OH_2)]OTf\cdot 0.5DCM$ ($C_{44.5}H_{70}CaClCoF_3N_4O_{16}S_4$): C, 43.22 (43.01); H, 5.70 (5.87); N, 4.53 (4.49)

Preparation of $[Co^{III}MST(\mu\text{-}OH)Ca\subset 15\text{-crown-}5]OTf$ from H_2O—$Me_4N[Co^{II}MST]$ (100 mg, 0.12 mmol) was suspended in 5 mL of THF and H_2O (12 mg, 0.67 mmol) was added, causing the mixture to become homogenous and pink. The solution was then treated with $[FeCp_2]OTf$ (40 mg, 0.12 mmol) to produce a dark red mixture that was stirred for at least 30 min. The mixture was then treated with a 1 mL THF solution containing the following species: $Ca^{II}[N(TMS)_2]_2(THF)_2$ (45 mg, 0.089 mmol), $Ca^{II}OTf_2$/15-crown-5 (50 mg, 0.090 mmol), and 15-crown-5 (20 mg, 0.091 mmol). This addition resulted in an immediate color change from dark red to yellow-brown. The solution was stirred for 1 h, after which it was filtered and the THF solvent was removed under reduced pressure. The brown solid was triturated with pentane (3×5 mL portions) until the washings were colorless, affording a yellow brown solid that was dried under reduced pressure. The solid was re-dissolved in a minimal amount of DCM and stored at −35°C overnight to produce a white solid (Me_4NOTf) and a small amount of pink crystals ($[Co^{II}MST(\mu\text{-}OH_2)Ca\subset 15\text{-crown-}5(OH_2)]OTf$) that were removed from the solution via filtration. The resulting yellow-brown filtrate was layered under pentane and stored at −35°C to produce yellow

NIH-PA Author Manuscript

NIH-PA Author Manuscript

NIH-PA Author Manuscript

brown crystals (44 mg, 31%). Crystals suitable for diffraction were obtained by dissolving the crystalline salt in DCM and layering under pentane at rt. FTIR: (KBr, cm^{-1}) ν(OH) 3430; selected vibrations 3023, 2935, 2858, 1604, 1471, 1405, 1380, 1355, 1265, 1229, 1133, 1090, 1053, 1031, 978, 954, 872, 852, 822. UV–vis: λ_{max} (DCM, nm (ε, $M^{-1}cm^{-1}$)) 390 (4800), 430 (shoulder), 730 (730). ESI-MS(+) Cald (m/z) (found) for $[Co^{III}MST(\mu\text{-}OH)Ca\subset 15\text{-crown-}5]^+$($C_{43}H_{66}CaCoN_4O_{12}S_3$): 1025.2798 (1025.2771)

Preparation of [Co^{III}MST(μ-OH)Ca⊂15-crow-n5]OTf from PhIO—$Me_4N[Co^{II}MST]$ (99 mg, 0.12 mmol) was dissolved in 5 mL of DCM, $Ca^{II}OTf_2$/15-crown-5 (68 mg, 0.12 mmol) was added and the mixture was stirred until homogenous. The blue solution was then treated with PhIO (51 mg, 0.23 mmol), causing the blue solution to slowly turn yellow-brown (30 min). Unreacted PhIO was removed by filtration and the resulting yellow brown filtrate was concentrated to dryness to afford a solid that was washed with pentane (3×10 mL). The solid was extracted with benzene (3×10 mL). The benzene solution was reduced to dryness in vacuo. The resulting fine yellow-brown solid was isolated using a fritted-glass funnel, washed with pentane, and dried to afford 120 mg (85%) of the desired salt. The spectroscopic data match those obtained for samples of the salt made by the previously described method.

Preparation of [$Co^{III}MST(OH_2)$]—$Me_4N[Co^{II}MST]$ (50 mg, 0.061 mmol) was dissolved in 5 mL of DCM and treated with water (5.0 mg, 0.28 mmol), causing a color change from blue to pink. The homogenous solution was treated with $[FeCp_2]OTf$ (42 mg, 0.13 mmol) resulting in an immediate color change to deep red. After stirring for 30 min, the reaction mixture was filtered and the DCM filtrate was layered under pentane. A brown-red solid mixture of $[Co^{III}MST(OH_2)]$, unreacted $[FeCp_2]OTf$, and Me_4NOTf was obtained, which was isolated on a fritted-glass funnel and washed with pentane until the washings were colorless. The solid was dried (45 mg) and suspended in ~10 mL of toluene, stirred for at least 1 h, and filtered to afford a red filtrate. Pentane (10 mL) was then added to the filtrate and the mixture was stored at −35°C, causing the precipitation of pure $[Co^{III}MST(OH_2)]$. The complex was isolated on a fritted-glass funnel, washed with pentane, and dried (13 mg, 28 %). Crystals suitable for diffraction were obtained by saturating a DCM:pentane solution with pure $[Co^{III}MST(OH_2)]$ and storing at −35°C for an extended period of time. FTIR: (KBr, cm^{-1}) ν(OH) 3308; selected vibrations 2970, 2936, 2867, 1603, 1564, 1469 1442, 1405, 1388, 1306, 1280, 1144, 1118, 1073, 1051, 1033, 983. UV–vis: λ_{max} (DCM, nm (ε, $M^{-1}cm^{-1}$)) 403 (5700), 494 (5100), 845 (750). Anal. Calcd (found) for $[Co^{III}MST(OH_2)]$ ·0.75 DCM ($C_{33.75}H_{48.5}Cl_{1.5}CoN_4O_7S_3$): C, 48.80 (49.07); H, 5.89 (6.32); N, 6.75 (6.72)

Physical Methods

Elemental analyses were performed on a Perkin-Elmer 2400 CHNS analyzer. Electronic absorbance spectra were recorded with a Cary 50 UV-vis spectrophotometer and an 8453 Agilent UV-vis spectrophotometer equipped with an Unisoku Unispeks cryostat. Fourier transform infrared spectra were collected on a Varian 800 Scimitar Series FTIR spectrometer. ^1H NMR spectra were recorded on a Bruker DRX500 spectrometer. High resolution mass spectra were collected using Waters Micromass LCT Premier Mass Spectrometer. Cyclic volt-ammetric experiments were conducted using a CHI600C electrochemical analyzer. A 2.0 mm glassy carbon electrode was used as the working electrode at scan velocities 0.1 $V{\cdot}s^{-1}$. A cobaltocenium/cobaltocene couple (−1.33 V vs. $[FeCp2]^{+/0}$) was used as an internal reference to monitor the reference electrode (Ag^+/Ag). Perpendicular-mode X-band electron paramagnetic resonance (EPR) spectra were collected using a Bruker EMX spectrometer equipped with an ER041XG microwave bridge, an ER4116DM dual-mode cavity, and an Oxford Instrument liquid He quartz cryostat. All EPR spectra were recorded at 10 K with the following experimental parameters: frequency 9.64

NIH-PA Author Manuscript

NIH-PA Author Manuscript

NIH-PA Author Manuscript

GHz, power 0.20 mW, modulation amplitude 9.02 G, time constant 20.48 seconds, conversion time 40.96 seconds. EPR spectral simulations were done using SpinCount 3.0.[12] Crystals for X-ray diffraction were mounted on a Bruker SMART APEX II diffractometer and the APEX2 program package was used to determine the unit-cell parameters and for data collection.[12] X-ray absorption spectra were collected at the Stanford Synchrotron Radiation Lightsource (SSRL) on beamlines 7–3 at an electron energy of 3.0 GeV with an average current of 300 mA The radiation was monochromatized by a Si(220) double-crystal monochromator. The intensity of the incident X-ray (I_0) was monitored by an N_2-filled ion chamber in front of the sample. The data were collected as fluorescence excitation spectra with a Ge 30 element detector (Canberra). Energy was calibrated by the rising edge position of Co foil (7709.0 eV).

RESULTS AND DISCUSSION

Sulfonamido groups have been used by others to prepare multidentate ligands. For instance, the work of Walsh illustrated that C_2 symmetric sulfonamido ligands could be used to synthesize a series of metal complexes.[13] Structural studies on these complexes showed that in some cases both the deprotonated nitrogen donors and the oxygen atoms could bind metal ions to form bridged dinuclear complexes. Sulfonamido groups also have been incorporated into tripodal compounds, but only those ligands of Mountford were used to prepare metal complexes.[14] We have extended the use of sulfonamido-based tripods by preparing $[MST]^{3-}$, which has allowed us to synthesize heterobimetallic complexes.[9] Formation of this type of complex takes advantage of the two structurally distinct metal ion-binding sites on the ligand (Chart 1): one that is composed of four nitrogen atoms and a second site that incorporates oxygen atoms of the sulfonamido moieties. The nitrogen-based site can readily bind a transition metal ion, whereas the oxygen-based site is able to bind main-group metal ions. Furthermore, the sulfonamido groups are positioned to promote the formation of intramolecular H-bonds. We have applied these concepts to assemble a series of Co^{II}–aquo and Co^{III}–OH complexes.

Preparation and Structure of $[Co^{II}MST]^-$

Treating a DMA solution of H_3MST with 3 equiv of KH followed by $Co^{II}(OAc)_2$ and metathesis with $Me_4N(OAc)$ resulted in the formation of $Me_4N[Co^{II}MST]$, which was purified via crystallization. The crystal structure of $Me_4N[Co^{II}MST]$ revealed that the anion contained a four-coordinate cobalt center having trigonal monopyramidal (TMP) coordination geometry (Figure 1). The average Co-N_{eq} bond length and N_{eq}-Co-N_{eq} angle were 1.967(3) Å and 119.1(2)°, and the Co1–N1 bond distance was 2.114(1) Å (Table 1). The Co^{II} center is displaced 0.207 Å from the plane formed by N2, N3, and N4 toward the vacant axial coordination site. These metrical parameters are similar to those of other Co^{II} complexes with TMP geometry.[15a,b;16] The structure of $[Co^{II}MST]^-$ also showed that the SO_2R groups of the $[MST]^{3-}$ ligand formed a cavity around the vacant coordination site on the cobalt center. The UV-vis spectrum of $Me_4N[Co^{II}MST]$ in DCM had absorbance peaks at λ_{max} = 410 nm, 572 nm and 712 nm (Figure S1)—these features are similar to the optical properties found for previously reported TMP Co^{II} complexes.[15a,b;16] Moreover, EPR spectra on frozen DCM solutions of $Me_4N[Co^{II}MST]$ showed that the complex has an S = 3/2 spin ground state (Table 2), similar to what is observed in other C_3-symmetric, four-coordinate Co^{II} complexes.[15b,17] Based on these data we concluded that $[Co^{II}MST]^-$ maintained a TMP structure in solution and could serve as a synthon for the preparation of $Co^{II/III}$–OH_2 and Co^{III}–OH complexes.

NIH-PA Author Manuscript

NIH-PA Author Manuscript

NIH-PA Author Manuscript

Preparation and Structures of Co^{II}–Aquo Complexes

The synthesis of $[Co^{II}MST]^-$ allowed us to examine the step-wise binding of external species to the complex. This process is illustrated with the preparation of the mono-aquo Co^{II} complex $[Co^{II}MST(OH_2)]^-$, which was accomplished by treating a DCM solution of $[Co^{II}MST]^-$ with excess H_2O causing a color change from sky blue to pink (Scheme 1). The UV-vis spectrum of $[Co^{II}MST(OH_2)]^-$ is similar to that found for the Co^{II}-OH complex $[Co^{II}H_3buea(OH)]^{2-}$, which has a TBP coordination geometry.[15c] The molecular structure of the complex was determined by X-ray diffraction methods and confirmed the trigonal bipyramidal coordination geometry of the cobalt center (Figure 2). The binding of the water molecule occurs at the open site within the sulfonamido cavity, having a Co1–O7 bond distance of 2.135(1) Å and an O7-Co1-N1 bond angle of 175.52(5)°. Minor structural differences in bond lengths of less than 0.085 Å were found between $[Co^{II}MST]^-$ and $[Co^{II}MST(OH_2)]^-$. In addition, the Co^{II} ion is displaced 0.310 Å from the plane formed by N2, N3, and N4 atom of $[MST]^{3-}$, a change of greater than 0.1 Å from that observed in $[Co^{II}MST]^-$. The aquo ligand also forms two intramolecular H-bonds to the O3 and O 5 atoms of $[MST]^{3-}$ as indicated by the O7···O3 and O7···O5 distances of 2.677(2) Å.

The binding of water to $[Co^{II}MST]^-$ also occurred when Ca^{II} ions were added to the complex. In the presence of $CaOTf_2$/15-crown-5 and 5 equiv H_2O (Scheme 1), a new species was isolated whose analytical and vibrational properties suggested the formation of a heterobimetallic complex containing a Co^{II}–(μ-OH_2)–Ca^{II} core. The visible spectrum of this species measured in DCM was similar to $[Co^{II}MST(OH_2)]^-$, a finding that is consistent with the complex maintaining a Co^{II}–aquo unit with trigonal bipyramidal coordination geometry (Figure S1).[18]

Determination of the molecular structure of this new species revealed the heterobimetallic complex $[Co^{II}MST(\mu\text{-}OH_2)Ca^{II}\subset 15\text{-crown-}5(OH_2)]^+$ ($[Co^{II}(\mu\text{-}OH_2)Ca^{II}OH_2]^+$) (Figure 3). As in $[Co^{II}MST(OH_2)]^-$, the Co^{II} ion accommodates a single aquo ligand; however, the aquo ligand bridges the Co^{II} and Ca^{II} ions to form the Co^{II}–(μ-OH_2)–Ca^{II} core. There are several small changes in the metrical parameters around the Co^{II} ion as compared to those in $[Co^{II}MST(OH_2)]^-$. For instance, the Co1–O7 bond length of 2.221(2) Å in $[Co^{II}(\mu\text{-}OH_2)Ca^{II}OH_2]^+$ is elongated by 0.086 Å. In addition, the Co^{II} ion in $[Co^{II}(\mu\text{-}OH_2)Ca^{II}OH_2]^+$ is slightly more displaced out of the trigonal plane by 0.015 Å. The bridging aquo ligand also forms two intramolecular H-bonds as indicated by the O7···O3 and O7···O5 distances of 2.656(2) Å and 2.693(2) Å. These changes suggested that the Ca^{II} ion does not perturb the primary coordination sphere of the Co^{II} ion to a large extent, in agreement with the optical spectrum.

In addition to the small changes in the primary coordination sphere of the Co^{II} center, there are several new structural features within the secondary coordination sphere. The $[Co^{II}MST(OH_2)]^-$ moiety acts as a bidentate ligand to the Ca^{II} ion through the bridging aquo O7 atom and the O1 atom from a sulfonamido group with a Ca1–O1 bond distance of 2.399(1) Å and a longer Ca1–O7 length of 2.531(2) Å. The structure of $[Co^{II}(\mu\text{-}OH_2)Ca^{II}OH_2]^+$ also showed that the complex had a second terminal aquo ligand bonded to the Ca^{II} ion. The Ca1–O13 bond length of 2.369(2) Å is significantly shorter than the distance observed for the Ca1–O7 bond by 0.16 Å. The terminal aquo also forms a single intramolecular H-bond with an O13···O2 distance of 2.758(2) Å. The oxygen atoms of the 15-crown-5 ligand fill the remaining coordination sites on the Ca^{II} ion. The structure of $[Co^{II}(\mu\text{-}OH_2)Ca^{II}OH_2]^+$ also showed that the two aquo ligands are relatively close to one another, having an O7···O13 interatomic distance of 3.762(3) Å.

Even though the structural properties of the primary coordination sphere of the Co^{II} center in $[Co^{II}MST(OH_2)]^-$ and $[Co^{II}(\mu\text{-}OH_2)Ca^{II}OH_2]^+$ are nearly the same, the addition of Ca^{II} ion

NIH-PA Author Manuscript

NIH-PA Author Manuscript

NIH-PA Author Manuscript

affects the lability of Co–OH_2 unit in the solid state. Conversion of $[Co^{II}MST(OH_2)]^-$ to $[Co^{II}MST]^-$ was accomplished by simply applying a small vacuum ($P \sim 10^{-3}$ torr). However, attempts to remove either the terminal or bridging aquo ligands in $[Co^{II}(\mu\text{-}OH_2)Ca^{II}OH_2]^+$ were unsuccessful, even after prolonged exposure to vacuum, determined by comparison of FTIR spectra (Figure S2B) and elemental analyses to those obtained from independently pre-pared samples of $[Co^{II}(\mu\text{-}OH_2)\text{-}Ca^{2+}\subset$15-crown-5-$(OH_2)]OTf$.

Electrochemical and EPR Properties

The redox properties of the Co^{II} complexes were explored using cyclic voltammetry in DCM (Figures 4A and S3, Table 2). For $[Co^{II}MST]^-$, a reversible one-electron process was observed at 0.41 V vs $[FeCp_2]^{+/0}$ that is assigned to the $Co^{II/III}$ couple. The potential shifted to more positive values when Ca^{II} ions were introduced to the electrochemical cell. Treating $[Co^{II}MST]^-$ with 1 equiv $Ca(OTf)_2$/15-crown-5 produced a new quasi-reversible couple at 0.62 V vs $[FeCp_2]^{+/0}$, suggesting that Ca^{II} ions can interact with $[Co^{II}MST]^-$ in the absence of an external ligand within the cavity (Figure S3).

The electrochemical properties of the Co^{II}–OH_2 complexes were substantially different from $[Co^{II}MST]^-$. For $[Co^{II}MST(OH_2)]^-$, a reversible couple was found at 0.068 V, a shift of nearly 0.4 V from that of $[Co^{II}MST]^-$. This shift is consistent with a more facile oxidation of a five-coordinate Co^{II} center than one that is four-coordinate. The $Co^{II/III}$ potential for $[Co^{II}(\mu\text{-}OH_2)Ca^{II}OH_2]^+$ appeared at 0.29 V vs. $[FeCp_2]^{+/0}$, a shift of more than 0.2 V compared to $[Co^{II}MST(OH_2)]^-$. The increase in redox potential reflects that change in overall positive charge of the complex upon the binding of the Ca^{II} ion.

The ⊥-mode EPR spectra measured on frozen solutions of the Co^{II} complexes all have features with *g*-values centered near 4.3 and 2.0, which is indicative of $S = 3/2$ spin ground states.[17] However, there are distinguishable differences in the *g*-values (Figures 4B and S4, Table 2) that reflect the changes in the coordination environments of the complexes. In addition, the complexes have similar eight-line hyperfine patterns on the features at $g \sim 2.0$ (Table 2), which is consistent with monomeric Co^{II} species. Notice that the largest difference in the hyperfine splitting ($\Delta A_z = 8 \times 10^{-4}$ cm^{-1}) is observed between the two Co^{II}–OH_2 species, $[Co^{II}MST(OH_2)]^-$ and $[Co^{II}(\mu\text{-}OH_2)Ca^{II}OH_2]^+$.

Synthesis & Structure of $[Co^{III}MST(OH_2)]$

The reversible $Co^{II/III}$ couple measured for $[Co^{II}MST(OH_2)]^-$ prompted our investigation into isolating this oxidized product by chemical methods. We found that treating $[Co^{II}MST(OH_2)]^-$ with $[Fe^{III}Cp_2]OTf$ in DCM (or THF) resulted in an immediate color change from pink to deep red (Scheme 1, Figure S5). The optical spectrum in DCM of the new species revealed intense features at λ_{max} (ε*M*) = 403 (5700), 494 (5100), 845 (750) nm that are characteristic of Co^{III} complexes with TBP geometry.[15c] Additional spectroscopic and analytical measurements suggested that this new red species was the expected Co^{III}–OH_2 complex, $[Co^{III}MST(OH_2)]$. We also investigated this oxidative process in the presence of $Ca(OTf)_2$/15-crown-5 and found that the reaction was incomplete when using $[Fe^{III}Cp_2]OTf$ as the oxidant, which agrees with our electrochemical observations. Complete conversion to an oxidized species was accomplished using the stronger oxidant acetyl ferrocenium tetrafluoroborate ($E_{1/2}$ = 0.27 V vs. $[FeCp_2]^{+/0}$);[11b] this complex had optical properties nearly identical to those of $[Co^{III}MST(OH_2)]$ but we were unable to obtain the complex in sufficient purity to determine its formulation.

The molecular structure of $[Co^{III}MST(OH_2)]$ showed that the primary coordination sphere of the cobalt center had the expected contraction compared to its Co^{II}–OH_2 analog (Table 1 and Figure S6). The Co1–N1 bond distance in $[Co^{III}MST(OH_2)]$ is 1.954(2) Å and its

NIH-PA Author Manuscript

NIH-PA Author Manuscript

NIH-PA Author Manuscript

average Co1–N_{eq} bond distance is 1.946 Å, which are shorter by 0.245 Å and 0.088 Å, respectively compared to those in $[Co^{II}MST(OH_2)]^-$. In addition, the Co1–O7 bond distance in $[Co^{III}MST(OH_2)]$ decreased by 0.201 Å upon oxidation to 1.934(2) Å. There are also intramolecular H-bonds between the aquo ligand and $[MST]^{3-}$ in $[Co^{III}MST(OH_2)]$, yet the O7···O1 and O7···O5 distances of 2.589 Å and 2.576 Å are significantly shorter than those found in $[Co^{II}MST(OH_2]^-$. The shortening of these distances corresponds to a strengthening of the H-bonds in $[Co^{III}MST(OH_2)]$, which is expected because the acidity of the aquo ligand will increase upon coordination to the Co^{III} center. This premise is further supported by FTIR studies: the ν(O-H) bands in $[Co^{III}MST(OH_2)]$ are broadened and at lower energies than those found in $[Co^{II}MST(OH_2)]^-$.

Oxidation Chemistry: Preparation and Structure of $[Co^{III}MST(\mu\text{-}OH)\text{-}Ca\subset 15\text{-}crown\text{-}5]^+$

$[Co^{II}MST]^-$ did not react with dioxygen even in the presence of Ca^{II} ions, in agreement with our electrochemical measurements. The reactivity of $[Co^{II}MST]^-$ with PhIO was also explored and we found no evidence for a reaction, even after several days. However, when $[Co^{II}MST]^-$ was treated with PhIO in the presence of $Ca(OTf)_2$/15-crown-5, a new dark yellow-brown species was formed within 1 h (Scheme 1). The new species had an absorption spectrum in DCM with features at λ_{max} (ε M) = 390 (4800), 430 (sh), 730 (730) nm, which are similar to another monomeric TBP Co^{III}–OH complex (Figure S5).[15c] ESI-HRMS results showed a species with a strong ion peak with mass-to-charge ratio (*m/z*) of 1025.2771 (calcd, 1025.2798) corresponding to a species having a formulation of $[Co^{III}MST(\mu\text{-}OH)\text{-}Ca\subset 15\text{-}crown\text{-}5]^+$ ($[Co^{III}(\mu\text{-}OH)Ca^{II}]^+$). Furthermore, FTIR analysis revealed a sharp peak at 3430 cm^{-1} supporting the presence of a hydroxo ligand (Figure S7).

Repeated attempts to crystallize $[Co^{III}(\mu\text{-}OH)Ca^{II}]^+$ synthesized from PhIO were unsuccessful and thus a new synthetic route was sought. We reasoned that deprotonation of $[Co^{III}MST(OH_2)]$ with an appropriate base could lead to a putative Co^{III}-OH complex which could then be treated with $Ca(OTf)_2$/15-crown-5 to form $[Co^{III}(\mu\text{-}OH)Ca^{II}]^+$. This approach was realized by treating a THF solution of $[Co^{III}MST(OH_2)]$ with 0.5 equiv $Ca[N(TMS)_2]_2{\cdot}THF_2$, 0.5 equiv 15 -crown-5, and 0.5 equiv $Ca(OTf)_2$/15-crown-5 that produced a species that had identical spectroscopic properties to $[Co^{III}(\mu\text{-}OH)Ca^{II}]^+$ (Scheme 1). Moreover, this approach yielded single crystals that were suitable for X-ray structural determination, thereby confirming the mass spectral formulation of the yellow-brown species as $[Co^{III}MST(\mu\text{-}OH)\text{-}Ca\subset 15\text{-}crown\text{-}5]^+$ (Figure 5). The molecular structure of $[Co^{III}(\mu\text{-}OH)Ca^{II}]^+$ contained a hydroxo ligand bridging the Co^{III} center and the Ca^{II} ion, in a manner similar to the manganese analog.[9] The Co^{III} center has TBP coordination geometry provided by the nitrogen donors of the $[MST]^{3-}$ ligand and the hydroxo ligand. The Co1–N1 and Co1–N_{eq} bond distances are comparable to those found for $[Co^{III}MST(OH_2)]$. However, the Co1–O7 bond distance in $[Co^{III}(\mu\text{-}OH)Ca^{II}]^+$ is 1.854(1) Å,[19] a decrease in length of 0.080 Å from $[Co^{III}MST(OH_2)]$ and 0.367 Å from $[Co^{II}(\mu\text{-}OH_2)Ca^{II}OH_2]^+$. The N1-Co1-O7 bond angle in $[Co^{III}(\mu\text{-}OH)Ca^{II}]^+$ is statistically equivalent to that in $[Co^{II}(\mu\text{-}OH_2)Ca^{II}OH_2]^+$, whereas the Ca1–O7 bond distance in $[Co^{III}(\mu\text{-}OH)Ca^{II}]^+$ is 0.265 Å shorter than that in $[Co^{II}(\mu\text{-}OH_2)Ca^{II}OH_2]^+$. In addition, there is a large contraction of the Co1-Ca1 interatomic distance of over 0.5 Å between $[Co^{II}(\mu\text{-}OH_2)Ca^{II}OH_2]^+$ and $[Co^{III}(\mu\text{-}OH)Ca^{II}]^+$.

A comparison of the molecular structures of $[Co^{II}(\mu\text{-}OH_2)Ca^{II}OH_2]^+$ and $[Co^{III}(\mu\text{-}OH)Ca^{II}]^+$ (Table 3) illustrate the versatility of the $[MST]^{3-}$ ligand to accommodate a second metal ion and form intramolecular H-bonds. In $[Co^{III}(\mu\text{-}OH)Ca^{II}]^+$ a single intramolecular H-bond between the hydroxo ligand and O5 of the $[MST]^{3-}$ ligand was present. Because of this lone H-bond, the remaining sulfonamido groups, along with the hydroxo ligand, formed a triden-tate-binding site for the calcium ion: binding to the Ca^{II} ion occurred through O7 and the O1 and O3 atoms of the sulfonamido groups. In $[Co^{II}(\mu\text{-}$

NIH-PA Author Manuscript

NIH-PA Author Manuscript

NIH-PA Author Manuscript

$OH_2)Ca^{II}OH_2]^+$, the bridging aquo ligand (the one containing O7) is involved in two intramolecular H-bonds with the $[MST]^{3-}$ ligand. Thus, the O1 atom of the remaining sulfonamido group and O7 act as a bidentate ligand to the calcium center. These results suggest that $[MST]^{3-}$ can regulate the mode of coordination to a second metal ion depending on the type of intramolecular H-bonding network in the complex.

The reactivity of $[Co^{III}(\mu\text{-}OH)Ca^{II}]^+$ with DPH was also explored. $[Co^{III}(\mu\text{-}OH)Ca^{II}]^+$ reacts slowly with 0.5 equiv of DPH at room temperature. However, when 10 equiv DPH were employed, $[Co^{III}(\mu\text{-}OH)Ca^{II}]^+$ was converted to a new species in less than 20 min, whose EPR spectrum was identical to that of $[Co^{II}(\mu\text{-}OH_2)Ca^{II}OH_2]^+$ (Figures S8 and S9), along with the formation of azobenzene in a yield of 70%.

Comparison of $[Co^{III}(\mu\text{-}OH)Ca^{II}]^+$ to a Proposed $[Co^{IV}(\mu\text{-}O)Sc^{III}]^{2+}$ Complex

We compared the properties of the $Co^{III/II}$ complexes with $[MST]^{3-}$ to other cobalt complexes with C_3-symmetric ligands.[10,15] In particular, we found noticeable similarities in the reactivity and physical properties to complexes synthesized by Ray derived from $[Co^{II}TMG_3tren(OTf)]^+$, a five-coordinate Co^{II} complex with a tripodal ligand that is comparable to $[MST]^{3-}$.[10] Both $[Co^{II}MST]^-$ and $[Co^{II}TMG_3tren(OTf)]^+$ are only oxidized with oxygen-atom transfer reagents in the presence of redox-inactive metal ions. Ray reported that treating $[Co^{II}TMG_3tren(OTf)]^+$ with $^{s}PhIO$ and $Sc(OTf)_3$ produced a new species formulated as $[(TMG_3tren)Co^{IV}(\mu\text{-}O)Sc^{III}(OTf)_3]^{2+}$, whose EPR features were assigned to a $Co^{IV}(\mu\text{-}O)Sc^{III}$ core having an $S = 3/2$ spin ground state. This presumed Co^{IV} product had a visible spectrum with features at λ_{max} = 489 and 810 nm that are strikingly similar to those found for $[Co^{III}(\mu\text{-}OH)Ca^{II}]^+$ (Figure S5) and other Co^{III}–O(H) species.[15c,d] Using EXAFS methods, a Co–O bond length of 1.85 Å was found in $[(TMG_3tren)Co^{IV}(\mu\text{-}O)Sc^{III}(OTf)_3]^{2+}$, which was used as evidence for a Co^{IV}–oxo unit; yet this bond length is identical to the Co1–O7 bond distance of 1.854(2) Å found by X-ray diffraction methods for $[Co^{III}(\mu\text{-}OH)Ca^{II}]^+$.[19] Moreover, data from X-ray absorption near-edge spectra (XANES) showed a 1.25 eV shift in edge energies between $[Co^{II}TMG_3tren]^{2+}$ and the $[(TMG_3tren)Co^{IV}(\mu\text{-}O)Sc^{III}(OTf)_3]^{2+}$ complex. The XANES spectra for both $[Co^{II}(\mu\text{-}OH_2)Ca^{II}OH_2]^+$ and $[Co^{III}(\mu\text{-}OH)Ca^{II}]^+$ have also been measured[20] (Figure 6) and we found an edge energy shift of 1.42 eV even though the cobalt centers in our complexes differ by only one oxidation state. From these results we propose that treating $[Co^{II}TMG_3tren(OTf)]^+$ with $^{s}PhIO$ in the presence of Sc^{3+} ions produced a meta-stable $[(TMG_3tren)Co^{III}(\mu\text{-}OH)Sc^{III}(OTf)_3]^{2+}$ complex rather than the Co^{IV}–oxo analog proposed previously. Our premise is supported by the similarities in the electronic and structural properties of the oxidized product of $[Co^{II}TMG_3tren(OTf)]^+$ with those found in other Co^{III}–hydroxo complexes, including $[Co^{III}(\mu\text{-}OH)Ca^{II}]^+$. A $[(TMG_3tren)Co^{III}(\mu\text{-}OH)Sc^{III}(OTf)_3]^{2+}$ complex should also have analogous types of reactivity as we observed for $[Co^{III}(\mu\text{-}OH)Ca^{II}]^+$; namely it can react with X–H bonds to produce a Co^{II}–containing species. Our proposal suggests that both Co^{III} and Co^{II} complexes could be present at the same time[21] and accounts for the observation of an $S = 3/2$ species (i.e., these EPR features are derived from a Co^{II} center, rather than Co^{IV}). Note that the EPR parameters, specifically the hyperfine interactions, between the putative Ray's Co^{IV}–oxo complex and our $[Co^{II}(\mu\text{-}OH_2)Ca^{II}OH_2]^+$ are nearly identical ($A_z = 100 \times 10^{-4}$ and 98×10^{-4} cm^{-1}, respectively).

SUMMARY

We have demonstrated for the first time the stepwise generation of Co–aquo complexes that led to the isolation of a system containing a $Co^{II}(\mu\text{-}OH_2)Ca^{II}OH_2$ core, a motif resembling structural elements found in the OEC. The active site includes both transition metal ions (Mn) and a Ca^{II} ion, in addition to an extensive H-bonding network, and all these features are critical for water oxidation.[3,4] The presence of a Ca^{II} ion in the OEC has prompted

NIH-PA Author Manuscript

NIH-PA Author Manuscript

NIH-PA Author Manuscript

several synthetic efforts to prepare transition metal clusters that include calcium ions.[5–9] In addition, intramolecular H-bonds have been proposed to be involved in some synthetic water oxidation systems[22] and have been used to isolate metal-aquo complexes.[23] However, incorporation of a Ca^{II} ion, transition metal ions, at least two water molecules, and an intramolecular H-bond network into a single molecular species has been difficult to replicate in synthetic systems. We accomplished the synthesis of this type of heterobimetallic complex using the multifunctional tripodal ligand $[MST]^{3-}$, which coordinated both Ca^{II} and Co^{II} ions, as it positioned two aquo ligands within 3 Å of each other. Its design took advantage of non-covalent interactions that linked the two metal centers and stabilized the aquo ligands through intramolecular H-bonds. Utilizing non-covalent interactions produced versatile systems in which the cobalt and Ca^{II} centers could readily adopt different primary and secondary coordination spheres.

Changes in redox properties of the Co^{II} complexes correlated with the coordination of Ca^{II} ions. For example, the redox potential of the $[Co^{II}MST]^-$ shifted over 200 mV in the presence of Ca^{II} ions. A similar positive shift was observed when Ca^{II} ions were added to $[Co^{II}MST(OH_2)]^-$. Moreover, $[Co^{II}MST]^-$ does not react with dioxygen but only stronger oxidants, such as PhIO, in the presence of Ca^{II} ions to afford the heterobimetallic complex $[Co^{III}(\mu\text{-}OH)Ca^{II}]^+$. The dependency of this reaction on Ca^{II} ions suggests an inner sphere process, whereby the Ca^{II} ion is essential for binding and oxidation. The need for Ca^{II} ions to promote reactivity is similar to what we observed in the synthesis of the analogous $[Mn^{III}(\mu\text{-}OH)Ca^{II}]^+$ species.[9,24]

The conversion of $[Co^{III}(\mu\text{-}OH)Ca^{II}]^+$ to $[Co^{II}(\mu\text{-}OH_2)Ca^{II}OH_2]^+$ when treated with DPH illustrated that Co^{III}–OH complexes can homolytically cleave X–H bonds. This type of reactivity is observed in the enzyme lipoxygenase which utilizes $Fe^{III}OH$ species to cleave C–H bonds.[2] Similar X–H bond cleavage reactivity by synthetic M^{III}–OH complexes are known,[25] but to our knowledge $[Co^{III}(\mu\text{-}OH)Ca^{II}]^+$ is the first example of a Co^{III}–OH species exhibiting this kind of chemistry. This finding, along with the structural and physical properties of $[Co^{III}(\mu\text{-}OH)Ca^{II}]^+$ and $[Co^{II}(\mu\text{-}OH_2)Ca^{II}OH_2]^+$, indicated that the recently reported Co^{IV}–oxo species[10] is actually a complex containing a Co^{III} center. Theoretical studies using DFT methods on *in silico*-generated Co^{IV}–oxo species suggest that the oxo ligand can have appreciable spin density,[10,26] leading to the possibility of Co^{III}–oxyl radical complexes. However, the existence of this type of species has yet to be validated experimentally. We think it is an unlikely assignment based on the data presented here, which is consistent with the more plausible formulation of a $Co^{III}(\mu\text{-}OH)Sc^{III}$ core.

Supplementary Material

Refer to Web version on PubMed Central for supplementary material.

Acknowledgments

We thank the NIH (GM50781) for support of this work. Portions of this research were supported by the Department of Energy (DOE), Office of Science, Office of Basic Energy Science (OBES), Division of Chemical Sciences, Geosciences and Biosciences, under contract DE-AC02–05CH11231, and carried out at the Stanford Synchrotron Radiation Lightsource (SSRL). SSRL is operated by DOE and OBES. The SSRL SMB Program is supported through DOE, OBER, and by the NIH, the National Center for Research Resources (NCRR).

ABBREVIATIONS

$[H_3buea]^{3-}$	tris(*tert*-butylureaylethylene)aminato
TMP	trigonal monopyramidal

NIH-PA Author Manuscript

NIH-PA Author Manuscript

NIH-PA Author Manuscript

TBP	trigonal bipyramidal
TBAP	tetrabutylammonium hexafluorophosphate
***d*[Co-N_{eq}]**	Co displacement from the equatorial plane formed by three deprotonated sulfonamido nitrogen donors of $[MST]^{3-}$
DPH	diphenylhydrazine
PhIO	iodosylbenzene
^{s}PhIO	2-(*tert*-butylsulfonyl)iodosylbenzene
ESI-HRMS	electrospray ionization high-resolution mass spectrometry
$N(TMS)_2$	bis(trimethylsilyl)amide
TMG_3tren	tris(tetramethylguanidino)tren

References

1. (a) Shook RL, Borovik AS. Inorg Chem. 2010; 49:3646–3660. [PubMed: 20380466] (b) Shook RL, Borovik AS. Chem Commun. 2008:6095–6107.(c) Borovik AS. Acc Chem Res. 2005; 38:54–61. [PubMed: 15654737] (d) Sigman JA, Kim HK, Zhao X, Carey JR, Lu Y. Proc Acad Natl Sci. 2003; 100:3629–3634.(e) Lu Y. Inorg Chem. 2006; 45:9930–9940. [PubMed: 17140190] (f) Lu Y, Yeung N, Sieracki N, Marshall NM. Nature. 2009; 460:855. [PubMed: 19675646] (g) Lu Y, Berry SM, Pfister TD. Chem Rev. 2001; 101:3047–f3080. [PubMed: 11710062] (h) Natale D, Mareque-Rivas JC. Chem Commun. 2008:425–437.
2. (a) Schurmann K, Anton M, Ivanov I, Richter C, Kuhn H, Walther M. J Biol Chem. 2011; 286:23920–23927. [PubMed: 21558275] (b) Saam J, Ivanov I, Walther M, Hozhütter HG, Kuhn H. Proc Natl Acad Sci. 2007; 104:13319–13324. [PubMed: 17675410] (c) Schenk G, Neidig ML, Zhou J, Holman TR, Solomon EI. Biochemistry. 2003; 42:7294–7302. [PubMed: 12809485]
3. Umena Y, Kawakami K, Shen J, Kamiya N. Nature. 2011; 473:55–61. [PubMed: 21499260]
4. (a) Barry BA, Chen J, Keough J, Jenson D, Offenbacher A, Pagba C. J Phys Chem Lett. 2012; 3:543–554. [PubMed: 22662289] (b) Saito K, Shen JR, Ishida T, Ishikita H. Biochemistry. 2011; 50:9836–9844. [PubMed: 21972783] (c) Haumann M, Junge W. Biochim Phys Acta. 1999; 1411:121–133.(d) Saito K, Shen JR, Ishida T, Ishikita H. Biochemistry. 2011; 50:9836–9844. [PubMed: 21972783] (e) Hwang HJ, Dilbeck P, Debus RJ, Burnap RL. Biochemistry. 2007; 46:11987–11997. [PubMed: 17915952] (f) Meyer TJ, Huynh MHV, Thorp H. H Angew Chem Int Ed. 2007; 46:5284–5304.(g) Polander BC, Barry BA. Proc Natl Acad Sci. 2012; 109:6112–6117. [PubMed: 22474345]
5. (a) Ghanotakis DF, Babcock GT, Yocum CF. FEBS Lett. 1984; 167:120–130.(b) Boussac A, Rutherford AW. Biochemistry. 1988; 27:3476–3483.(c) Ananyev GA, Zaltsman L, Vasko C, Dismukes GC. Biochim Biophys Acta. 2001; 1503:52–68. [PubMed: 11115624] (d) Yocum CF. Coord Chem Rev. 2008; 252:296–305.e) Miqyass M, Gorkom HJ, van Yocum CF. Photosynth Res. 2007; 92:275–287. [PubMed: 17235491] (f) Miqyass, M.; Yocum, CF.; van Gorkom, HJ. Calcium Requirements for S-State Transitions. In: Allan, JF.; Gantt, E.; Golbeck, JH.; Osmond, B., editors. Photosynthesis Energy from the Sun. Springer; Netherlands: 2008. p. 459-462.(g) Pecoraro VL, Baldwin MJ, Caudle MT, Hsieh WY, Law NA. Pure Appl Chem. 1998; 70:925–929.(h) Cady CW, Crabtree RH, Brudvig GW. Coord Chem Rev. 2008; 252:444–455. [PubMed: 21037800] (i) Brudvig GW. Philos Trans R Soc, B. 2008; 8:1211–1219.(j) Mullins CS, Pecoraro VL. Coord Chem Rev. 2008; 47:1849–1861.(k) Betley TA, Wu Q, Van-Voorhis T, Nocera DG. Inorg Chem. 2008; 47:1894–1861.
6. (a) Wiechen M, Zaharieva I, Dau H, Kurz P. Chem Sci. 201210.1039/C2SC20226C(b) Kanan MW, Nocera DG. Science. 2008; 321:1072–1075. [PubMed: 18669820] (c) Reece SY, Hamel JA, Sung K, Jarvi TD, Esswein AJ, Pijpers JJH, Nocera DG. Science. 2011; 334:645–648. [PubMed: 21960528]

NIH-PA Author Manuscript NIH-PA Author Manuscript NIH-PA Author Manuscript

7. (a) Kotzabasaki V, Siczek M, Lis T, Milios CJ. Inorg Chem Commun. 2011; 14:213–216.(b) Nayak S, Nayek HP, Dehnen S, Powell AK, Reedijk J. Dalton Trans. 2011; 40:2699–2702. [PubMed: 21327234] (c) Hewitt IJ, Tank J-K, Madu NT, Clérac R, Buth G, Anson CE, Powell AK. Chem Commun. 2006:2650–2652.(d) Mishra A, Wernsorfer W, Abboud KA, Christou G. Chem Commun. 2005:54–56.
8. Kanady JS, Tsui EY, Day WM, Agapie T. Science. 2011; 333:733–736. [PubMed: 21817047]
9. Park YJ, Ziller JW, Borovik AS. J Am Chem Soc. 2011; 133:9258–9261. [PubMed: 21595481]
10. Pfaff FF, Kundu S, Risch M, Pandian S, Heims F, Pry-jomska-Ray I, Haack P, Metzinger R, Bill E, Dau H, Comba P, Ray K. Angew Chem Int Ed. 2011; 50:1711–1715.
11. (a) Margulieux GW, Weidermann N, Lacy DC, Moore CE, Rheingold AL, Figueroa JS. J Am Chem Soc. 2010; 132:5033–5035. [PubMed: 20302355] (b) Connelly NG, Geiger WE. Chem Rev. 1996; 96:877–910. [PubMed: 11848774] (c) Panda TK, Hrib CG, Jones PG, Jenter J, Roesky PW, Tamm M. Eur J Inorg Chem. 2008:4270–4279.(d) Dauban P, Saniere L, Tarrade A, Dodd R. H J Am Chem Soc. 2001; 123:7707–7708.
12. See supporting information for experimental details
13. (a) Walsh PJ. Acc Chem Res. 2003; 36:739–749. [PubMed: 14567707] (b) Walsh PJ, Lurain AE, Balsells J. Chem Rev. 2003; 103:3297–3344. [PubMed: 12914499] (c) Pritchett S, Woodmansee DH, Gantzel P, Walsh PJ. J Am Chem Soc. 1998; 120:6423–6424.(d) Nanthakumar A, Miura J, Diltz S, Lee CK, Aguirre G, Ortega F, Ziller JW, Walsh PJ. Inorg Chem. 1999; 38:3010–3013. [PubMed: 11671053]
14. (a) Schwarz AD, Chu Z, Mountford P. Organometallics. 2010; 29:1246–1260.(b) Schwarz AD, Herbert KR, Paniagua C, Mountford P. Organometallics. 2010; 29:4171–4188.
15. (a) Ray M, Hammes BS, Yap GPA, Rheingold AL, Borovik AS. Inorg Chem. 1998; 37:1527–1532.(b) Lucas RL, Zart MK, Murkerjee J, Sorrell TN, Powell DR, Borovik AS. J Am Chem Soc. 2006; 128:15476–15489. [PubMed: 17132015] (c) Hammes BS, Young GV Jr, Borovik AS. Angew Chem Int Ed. 1999; 38:666–669.(d) Larsen LP, Parolin TJ, Powell DR, Hendrich MP, Borovik AS. Angew Chem Int Ed. 2003; 42:85–89.
16. (a) Ciampolini, M. Spectra of 3d Five-Coordinate Complexes. In: Jorgenen, CK.; Neilands, JB.; Nyholm, RS.; Reinen, D.; Williams, RJP., editors. Structure and Bonding. Vol. 6. Springer-Verlag; New York: 1969. p. 52-93.(b) Ciampolini M, Paoletti P. Inorg Chem. 1967; 6:1261–1262. (c) Suh MP, Lee J, Han MY, Yoon TS. Inorg Chem. 1997; 36:5651–5654.(d) Vaira MD, Orioli PL. Inorg Chem. 1967; 6:955–957.
17. (a) Banci, L.; Bencini, A.; Benelli, C.; Bohra, R.; Dance, J-M.; Gatteschi, D.; Jain, V.; Mehrotra, R.; Tressaud, A.; Woolley, R.; Zanchini, C. In Structures Versus Special Properties, Structure and Bonding. Vol. 52. Springer Berlin; Heidelberg: 1982. Spectral-Structural Correlations in High-Spin Cobalt(II) Complexes; p. 37-86.(b) Jenkins DM, Bilio AJD, Allen MJ, Betley TA, Peters J. C J Am, Chem Soc. 2002; 124:15336–15350.
18. We have spectrophotometrically monitored the formation of this Co^{II}-aquo species and found changes in the optical spectrum until one equiv of water was added to $[Co^{II}MST]^{-}$ and $Ca^{II}(OTf)_2$/15-crown-5; further addition of water caused no changes in the optical properties. Because we are only monitoring changes at the Co^{II} center, these findings suggest that only one water molecule affect the electronic transitions of the Co^{II} center (Figure S2), similar to what was observed for $[Co^{II}MST(OH_2)]^{-}$. However, these spectral data do not allow us to determine the exact structure of the complex in solution, in particular, the coordination spheres around the Ca^{II} center.
19. This bond distance is comparable to the Co^{III}–O bond length of 1.894(2) Å reported for the monomeric $[Co^{III}H_3buea(OH)]^{-}$.[15c] However, this bond distance is longer than the average Co^{III}–O bond length found in a homobimetallic Co^{III} complex with a $Co^{III}_2(\mu\text{-}O)_2$core.[15d]
20. (a) The edge energies determined from the 2nd derivative of the XANES spectra are 7716.40 eV for $[Co^{II}(\mu\text{-}OH_2)Ca^{II}OH_2]^{+}$ and 7717.82 eV for $[Co^{III}(\mu\text{-}OH)Ca^{II}]^{+}$Bonnitcha PD, Hall MD, Underwood CK, Foran GJ, Zhang M, Beale PJ, Hambley T. W J Inorg Biochem. 2006; 100:963–971.Kanan MW, Yano J, Surendranath Y, Dincâ M, Yachandra VK, Nocera D. G J Am Chem Soc. 2010; 132:13692–13701.
21. The kinetics of this reaction would allow for both the Co^{III}– OH and Co^{II}–OH_2 species to be present at the same time.

NIH-PA Author Manuscript

NIH-PA Author Manuscript

NIH-PA Author Manuscript

22. (a) Dogutan DK, McGuire R Jr, Nocera D. J Am Chem Society. 2011; 133:9178–9180.(b) Dogutan DK, Stoian SA, McGuire R Jr, Schwalbe M, Teets TS, Nocera D. G J Am Chem Soc. 2011; 133:131–140.(c) Boyer JL, Polyansky DE, Szalda DJ, Zong R, Thummel RP, Fujita E. Angew Chem Int Ed. 2011; 50:12600–12604.

23. Mareque-Rivas JC, Prabaharan R, Rosales RTM. Chem Commun. 2004:76–77.

24. Selected examples of the importance of redox-inactive metal ions on processes involving transition metal complexes: Fukuzumi S, Ohkubo K. Chem Eur J. 2000; 6:4532–4535. [PubMed: 11192086] Ohkubi K, Menon SC, Orita A, Otera J, Fukuzumi S. J Org Chem. 2003; 68:4720–4726. [PubMed: 12790575] Darensbourg MY, Darensbourg DJ, Burns D, Drew D. A J Am Chem Soc. 1976; 98:3127–3136.Gambarotta, Francesco A, Floriani C, Zanazzi PF. J Am Chem Soc. 1982; 104:5082–5092.Lee Y, Mankad NP, Peters JC. Nature Chem. 2010; 2:558–565. [PubMed: 20571574] Betley TA, Peters J. C J Am Chem Soc. 2003; 125:10782–10783.Ding K, Brennessel WW, Holland PL. J Am Chem Soc. 2009; 131:10804–10805. [PubMed: 19621923] Ding K, Pierpont AW, Brennessel WW, Lukat-Rodgers G, Rodgers KR, Cundari TR, Bill E, Holland P. L J Am Chem Soc. 2009; 131:9471–9472.Morimoto Y, Kotani H, Park J, Lee Y-M, Nam W, Fukuzumi S. J Am Chem Soc. 2011; 133:403–405. [PubMed: 21158434] Fukuzumi S, Morimoto Y, Kotani H, Naumov P, Lee YM, Nam W. Nature Chem. 2010; 2:756–759. [PubMed: 20729896] Karlin KD. Nature Chem. 2010; 2:711–712. [PubMed: 20729888]

25. (a) Goldsmith CR, Cole AP, Stack TDP. J Am Chem Soc. 2005; 127:9904–9912. [PubMed: 15998097] (b) Goldsmith CR, Stack TDP. Inorg Chem. 2006; 45:6048–6055. [PubMed: 16842013] (c) Donoghue PJ, Tehranchi J, Cramer CJ, Sarangi R, Solomon EI, Tolman WB. J Am Chem Soc. 2011; 133:17602–17605. [PubMed: 22004091] (e) Ogo S, Wada S, Watanabe Y, Iwase M, Wada A, Harata M, Jitsukawa K, Masuda H, Einaga H. Angew Chem Int Ed. 1998; 37:2102–2104.(e) Ogo S, Yamahara R, Roach M, Suenobu T, Aki M, Ogura T, Kitagawa T, Masuda H, Fukuzumi S, Watanabe Y. Inorg Chem. 2002; 41:5513–5520. [PubMed: 12377047]

26. Michel C, Baerends EJ. Inorg Chem. 2009; 48:3628–3638. [PubMed: 19301854]

NIH-PA Author Manuscript

NIH-PA Author Manuscript

NIH-PA Author Manuscript

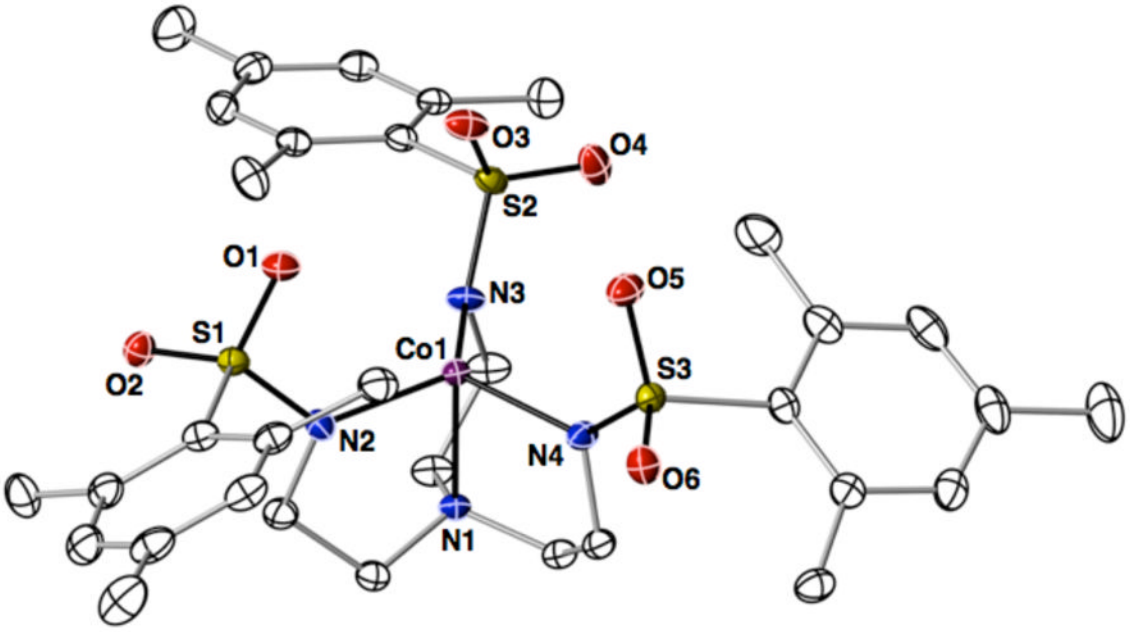

Figure 1.
Thermal ellipsoid diagram depicting the molecular structure of $[Co^{II}MST]^{-}$. The thermal ellipsoids are drawn at the 50% probability level and the hydrogen atoms are removed for clarity.

NIH-PA Author Manuscript

NIH-PA Author Manuscript

NIH-PA Author Manuscript

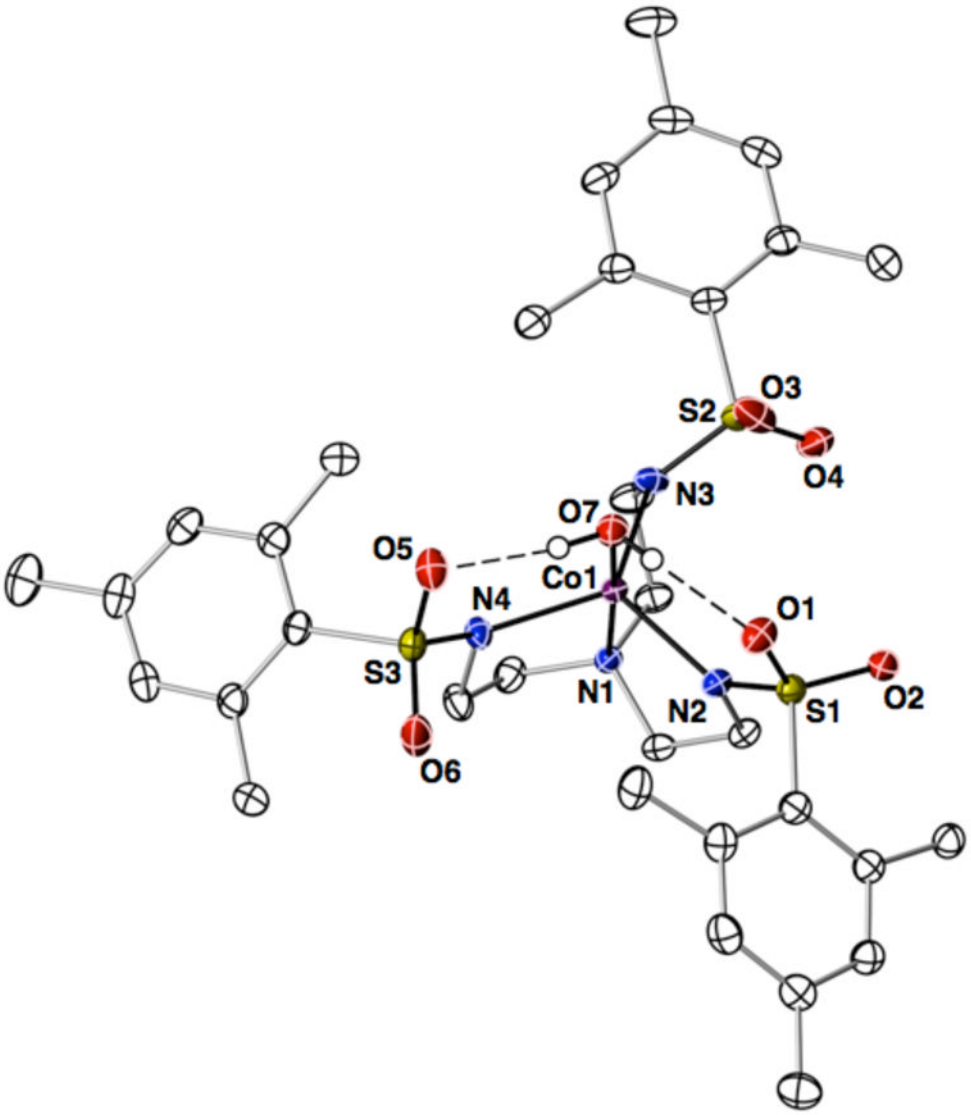

Figure 2.
Thermal ellipsoid diagram depicting the molecular structure of $[Co^{II}MST(OH_2)]^-$. The thermal ellipsoids are drawn at the 50% probability level and only the hydrogen atoms of the water ligand are shown for clarity.

NIH-PA Author Manuscript

NIH-PA Author Manuscript

NIH-PA Author Manuscript

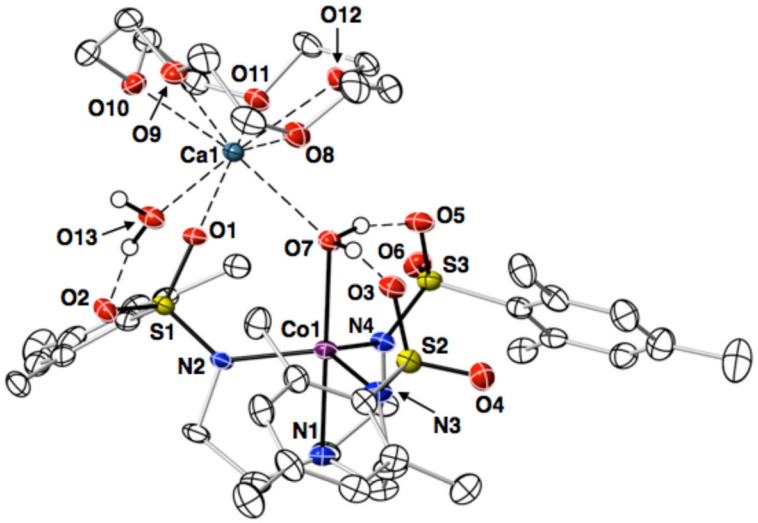

Figure 3.

Thermal ellipsoid diagram depicting the molecular structure of $[Co^{II}(\mu\text{-}OH_2)Ca^{II}OH_2]^+$. The thermal ellipsoids are drawn at the 50% probability level and only the hydrogen atoms of the water ligands are shown for clarity.

NIH-PA Author Manuscript

NIH-PA Author Manuscript

NIH-PA Author Manuscript

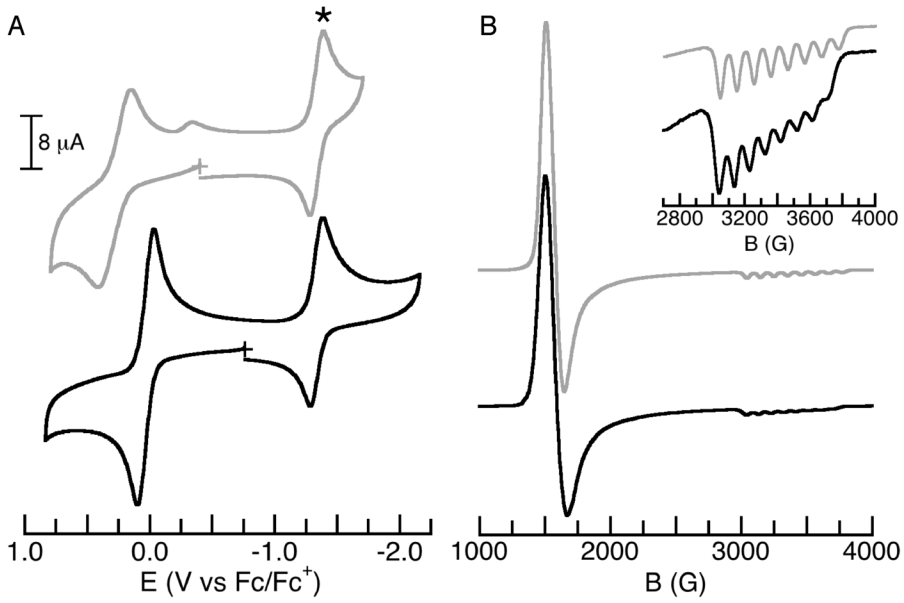

Figure 4.

Cyclic voltammograms (A) and ⊥-mode EPR spectra (B) of $[Co^{II}MST(OH_2)]^-$ (black line) and $[Co^{II}(\mu\text{-}OH_2)Ca^{II}OH_2]^+$ (gray line). Cobaltocenium (*) was used as an internal standard in the CV experiments. The voltammograms were recorded at room temperature in DCM (with 0.1 M $TBAPF_6$) and the EPR data were collected at 10 K on frozen DCM solution (6 mM). Inset: comparison of the hyperfine interactions for the two Co^{II}–aquo complexes. See Table 2 for $E_{1/2}$, g- and A_z-values.

NIH-PA Author Manuscript

NIH-PA Author Manuscript

NIH-PA Author Manuscript

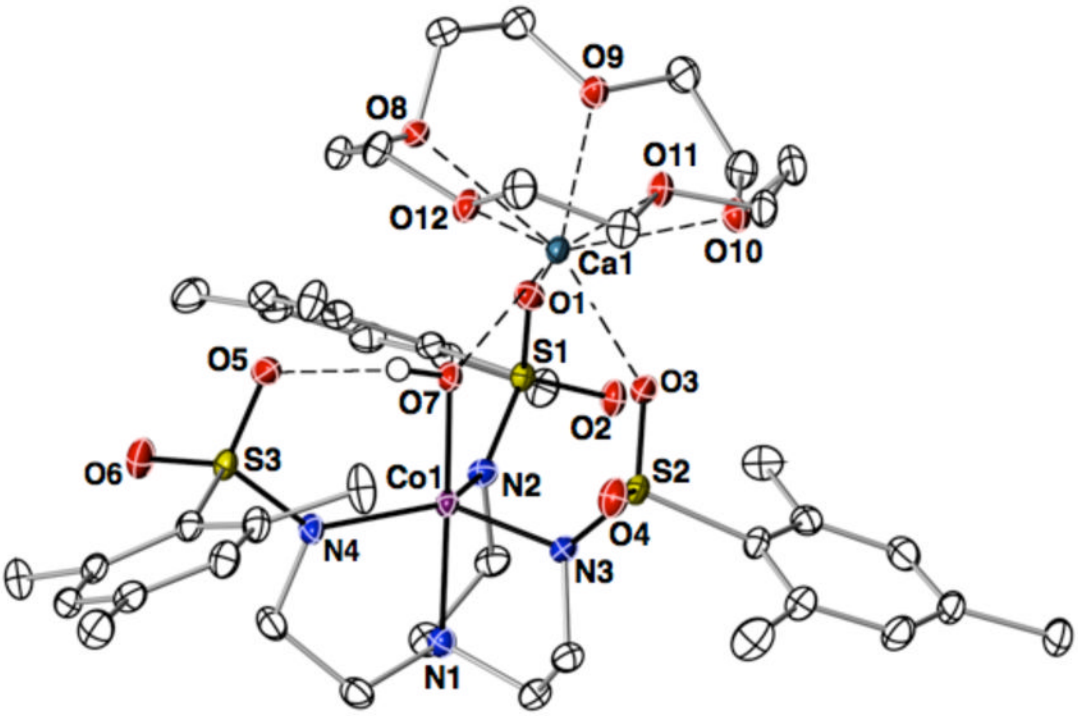

Figure 5.
Thermal ellipsoid diagram depicting the molecular structure of $[Co^{III}(\mu\text{-}OH)Ca^{II}]^{+}$. The thermal ellipsoids are drawn at the 50% probability level and only the hydrogen atom of the hydroxo ligand is shown for clarity.

NIH-PA Author Manuscript
NIH-PA Author Manuscript
NIH-PA Author Manuscript

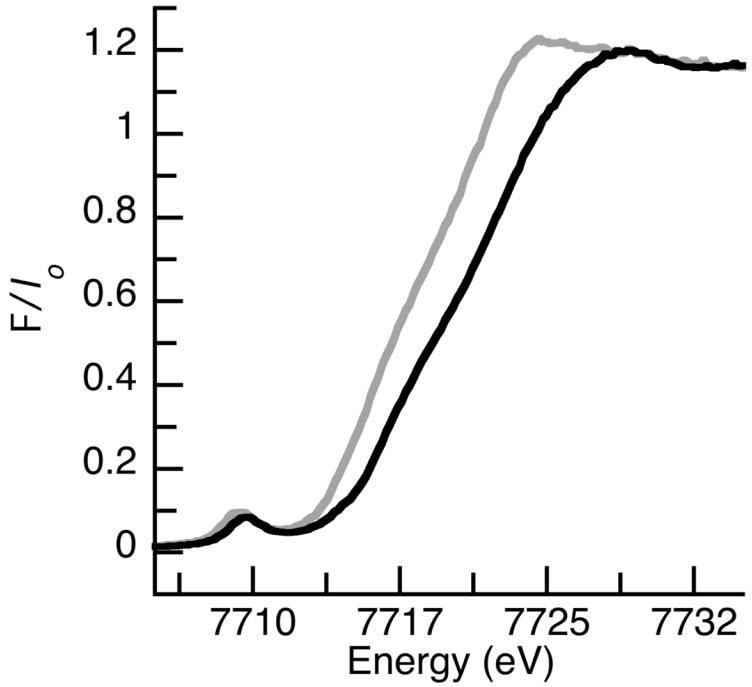

Figure 6.
XANES spectra for $[Co^{II}(\mu\text{-}OH_2)Ca^{II}OH_2]^+$ (gray line) and $[Co^{III}(\mu\text{-}OH)Ca^{II}]^+$ (black line) collected on solid samples (10% by weight) in boron nitride.[20]

NIH-PA Author Manuscript

NIH-PA Author Manuscript

NIH-PA Author Manuscript

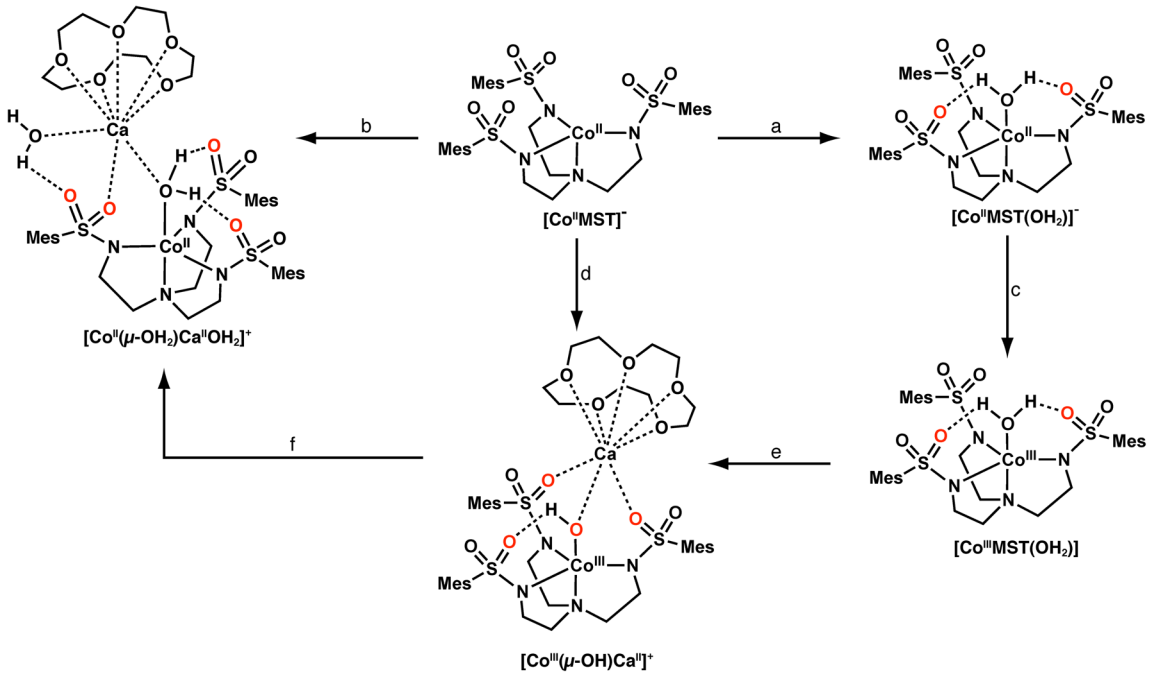

Scheme 1.

Preparative routes to the cobalt complexes. Conditions: a) 5–10 equiv H_2O, rt, DCM; b) $Ca(OTf)_2$/15-crown-5, 5 equiv H_2O, rt, DCM; c) [$Fe^{III}Cp_2$]OTf, rt, DCM (or THF); d) $Ca(OTf)_2$/15-crown-5, PhIO, rt, DCM; e) 0.5 equiv $Ca[N(TMS)_2]_2{\cdot}THF_2$, 0.5 equiv 15-crown-5, and equiv 0.5 $Ca(OTf)_2$/15-crown-5, rt, THF; f) 10 equiv DPH, rt, DCM.

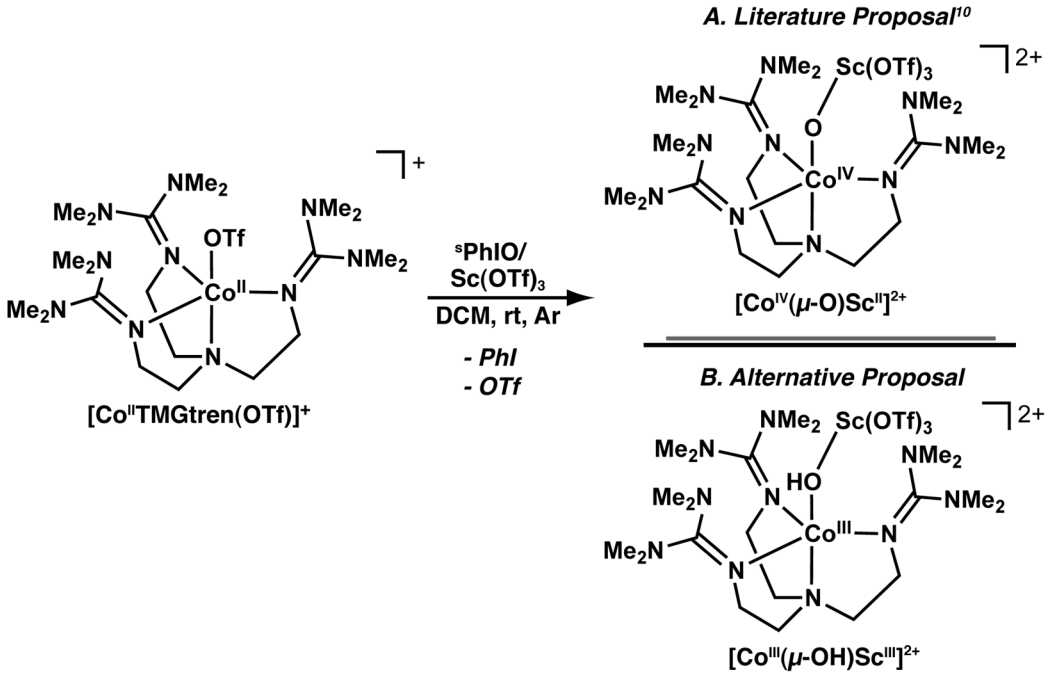

Scheme 2.

Comparison of possible heterobimetallic complex formed when treating $[Co^{II}TMGtren(OTf)]^{+}$ with $^{s}PhIO$ and $Sc(OTf)_3$ as proposed in the literature[10] (A) and reformulated based on the results obtained herein (B).

NIH-PA Author Manuscript NIH-PA Author Manuscript NIH-PA Author Manuscript

NIH-PA Author Manuscript

NIH-PA Author Manuscript

NIH-PA Author Manuscript

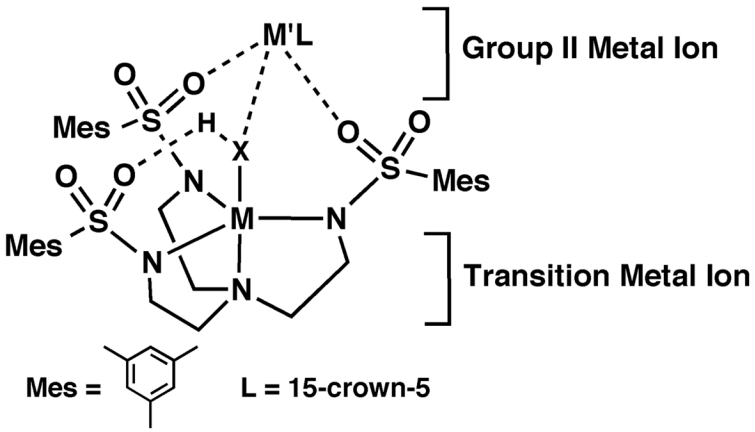

Chart 1.
Design Aspects of the Heterometallic Complexes.

NIH-PA Author Manuscript

NIH-PA Author Manuscript

NIH-PA Author Manuscript

Table 1

Selected metrical data for $[Co^{II}MST]^{-}$, $[Co^{II}MST(OH_2)]^{-}$, and $[Co^{III}MST(OH_2)]$.

	$[Co^{II}MST]^{-}$	$[Co^{II}MST(OH_2)]^{-}$	$[Co^{III}MST(OH_2)]$
		Bond Distances (Å)	
Co1–O7	NA	2.135(1)	1.934(2)
Co1–N1	2.114(1)	2.199(1)	1.954(2)
Co1–N2	1.973(1)	2.020(1)	1.950(2)
Co1–N3	1.957(1)	2.028(1)	1.927(2)
Co1–N4	1.971(1)	2.054(1)	1.961(2)
d[Co-N_{eq}]	0.207	0.310	0.127
		Bond Angles (°)	
N1-Co1-O7		175.52(5)	178.20(7)
N3-Co1-N4	118.90(5)	119.83(5)	119.48(8)
N4-Co1-N2	117.52(5)	119.28(5)	119.43(7)
N3-Co1-N2	120.31(5)	114.04(5)	118.78(7)

NIH-PA Author Manuscript

NIH-PA Author Manuscript

NIH-PA Author Manuscript

Table 2

EPR and Redox Properties of the Co^{II} Complexes.

Complex	*g*-values	A_z (cm^{-1})	$E_{1/2}$ (V)[a]
$[Co^{II}MST]^-$	4.36, 2.00	96×10^{-4}	0.41
$[Co^{II}MST]^-+Ca^{II}$	4.31, 2.00	94×10^{-4}	0.62
$[Co^{II}MST(OH_2)]^-$	4.33, 2.04	90×10^{-4}	0.068
$[Co^{II}(\mu\text{-}OH_2)Ca^{II}OH_2]^+$	4.35,2.02	98×10^{-4}	0.29

[a] versus $[FeCp_2]^{+/0}$

NIH-PA Author Manuscript

NIH-PA Author Manuscript

NIH-PA Author Manuscript

Table 3

Comparison of metrical parameters for $[Co^{III}(\mu\text{-}OH)Ca^{II}]^{+}$ and $[Co^{II}(\mu\text{-}OH_2)Ca^{II}OH_2]^{+}$.

	$[Co^{III}(\mu\text{-}OH)Ca^{II}]^{+}$	$[Co^{II}(\mu\text{-}OH_2)Ca^{II}OH_2]^{+}$
Bond Distances (Å)		
Co1–O7	1.854(1)	2.221(2)
Co1–N1	1.997(1)	2.126(2)
Co1–N2	1.971(2)	2.037(2)
Co1–N3	1.950(2)	2.031(2)
Co1–N4	1.962(2)	2.013(2)
Ca1–O1	2.361(2)	2.399(1)
Ca1–O3	2.379(1)	–
Ca1–O7	2.266(1)	2.531(2)
Ca1–O13	–	2.369(2)
Ca1···Co1	3.804(1)	4.315(1)
d[Co-N_{eq}]	0.212	0.325
Bond Angles (°)		
N1-Co1-O7	177.38(6)	177.75(7)
Co1-O7-Ca1	134.56(7)	130.41(7)
O7-Ca1-O13	–	100.29(6)
N3-Co1-N4	124.35(7)	113.87(8)
N4-Co1-N2	123.14(7)	11414(8)
N3-Co1-N2	109.01(7)	12440(8)